Disclaimer

The report at hand was written in the course of the respective class at the University of Bonn. If not stated differently on top of the first page or the following website, the report was prepared and handed in solely by me, Marvin Zanke. Any handwritten annotations are usually corrections that I or a tutor made. For more information and all my material, check: https://www.physics-and-stuff.com/

I raise no claim to correctness and completeness of the given report! This equally applies to the corrections mentioned above.

Advanced Laboratory Course

K225: Positron Lifetime in Metals and Insulators

Group P8

Marvin Zanke
s6mazank@uni-bonn.de

Fabian Müller
s6fnmuel@uni-bonn.de

September 11, 2018

Contents

Abstract

In this experiment, we consider the positron and its lifetime in metals. We investigate how positrons can be created and set up an experiment such that we can measure the lifetime until its annihilation. We study how to measure the time at which a positron is created and annihilated using a so-called fast-slow-coincidence circuit. To this end, we adjust a slow circuit, as well as a fast circuit and do a time calibration measurement.

Having adjusted and calibrated the experimental set up, we measure the positron lifetime spectra in ^{155}In for different temperatures. The positrons we use are created in a β^+-decay of ^{22}Na. The scintillator material used in this experiment contains ^{176}Lu, which is radioactive and emits positrons as well. From the measured spectra, we obtain the formation of vacancies' temperature dependence and determine the vacancy formation enthalpy.

1 Theory

If not mentioned explicitly, the theory is based on the references [1] and [2].

1.1 Positrons and their Lifetimes

1.1.1 The Positron and Positron Sources

The antiparticle of the electron is called *positron* and has the same physical properties such as mass $m_e = 511\,\text{keV}$ and spin $s_e = 1/2$ but an opposite charge of $Q_{e^+} = +e$. Positrons can be produced in various ways, one of these being the β^+-*decay* of radioactive isotopes, e.g. ^{22}Na in this experiment. Here, the advantage is that it mostly decays into an *excited state of* ^{22}*Ne* and emits an *additional photon* of energy $E_\gamma = 1.274\,\text{MeV}$ upon relaxation. As shall become clear later, this photon can be used as a start signal to measure the lifetime of the positron. The decay scheme of ^{22}Na is depicted in figure 1.1.1.

1.1.2 Positronium

In some materials, the positron and electron can form a stable state called *positronium (ps)*. It is a bound state like the hydrogen atom but with a binding energy of

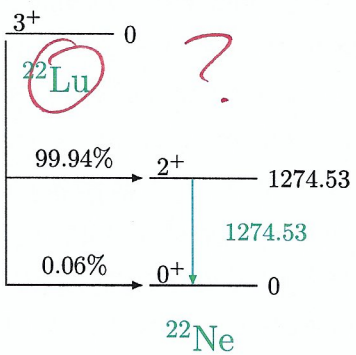

Figure 1.1.: The decay scheme of ^{22}Na into ^{22}Ne, following [1].

$E_B = -6.8\,\text{eV}$. In general, this will not happen in metals. The spins of the positron and electron can either be aligned parallel (ortho-ps) or antiparallel (para-ps). The o-ps lives much longer than the p-ps (~ns compared to ~ps).

1.1.3 Positron Annihilation

When a positron and an electron collide, they can *annihilate* and convert their mass into energy in form of photons. The *rest mass* of the both particles together equals $E_{e^-e^+} = 1.022\,\text{MeV}$ and is shared among a variable amount of photons, depending on the spins of the two particles (parallel or antiparallel). While the events with antiparallel spins can only decay into an even number of photons, the events with parallel spins can only decay into an odd number of photons. Former are dominated by a 2γ-*emission* and latter by a 3γ-*emission*. Each additional photon reduces the cross section by the fine structure constant $\alpha = 1/137$ as becomes clear when considering the feynman rules. Besides this *free annihilation*, they can also annihilate when already bound in positronium. Here, the p-ps decays through 2γ and the o-ps through 3γ. If the positronium is formed in the vicinity of atoms, the lifetime of the o-ps can be reduced by a so-called *pick-off process*. Here, the positron of the bound state annihilates with an electron of opposite spin in the material via a 2γ-decay. Another possible reduction in lifetime can be achieved due to a *quenching process*, turning o-ps into p-ps which then annihilates.

1.1.4 Positron states in Matter and Trapping model

Studying the behavior of positrons in matter, one can find useful information on the the properties of the material, e.g. *electronic properties and vacancies/defect structures*. For this purpose, the *lifetime spectra* of the positron come in handy.

After injecting energetic positrons into a solid they *thermalize*, which means they lose their energy (~eV remain) by ionizing collisions (~ps). Being in a so-called *free* state, they can move freely through the lattice of the material. A vacancy in this lattice is a missing ion at some position, which attracts the positron due to the lower potential. A positron filling such a vacancy is referred to as being *trapped*. Due to the lower electron density close to a vacancy, the probability of an annihilation is lower, making the lifetime of a trapped positron larger compared to a free one. Once trapped, a positron can not escape during its lifetime. A simple model describing this trapping for one type of vacancy is based on the two coupled

differential equations

$$\begin{aligned} \frac{\mathrm{d}n_\mathrm{f}}{\mathrm{d}t} &= -\lambda_\mathrm{f} n_\mathrm{f} - \kappa n_\mathrm{f}, \\ \frac{\mathrm{d}n_\mathrm{t}}{\mathrm{d}t} &= -\lambda_\mathrm{t} n_\mathrm{t} + \kappa n_\mathrm{f}, \end{aligned} \tag{1.1}$$

where n_f and n_t are the probabilities for a free or trapped positron as well as λ_f and λ_t their decay rates respectively. Furthermore, $\kappa = \sigma c_\mathrm{t}$ is the so-called trapping rate, where

$$c_\mathrm{t}(T) = \exp\left(\frac{S_\mathrm{t}}{k_\mathrm{B}} - \frac{H_\mathrm{t}}{k_\mathrm{B}T}\right) \tag{1.2}$$

with the temperature T, Boltzmann constant k_B, the vacancy formation entropy S_t and the vacancy formation enthalpy H_t. It is handy to introduce $\lambda_0 = \lambda_\mathrm{f} + \kappa$. Instead of the decay rates λ_i, one often uses the lifetimes $\tau_i = 1/\lambda_i$. Solving the differential equations, one arrives at the total decay rate

$$W(t) = -\frac{1}{n_0}\frac{\mathrm{d}n}{\mathrm{d}t} = \frac{I_0}{\tau_0}\exp\left(-\frac{t}{\tau_0}\right) + \frac{I_\mathrm{t}}{\tau_\mathrm{t}}\exp\left(-\frac{t}{\tau_\mathrm{t}}\right). \tag{1.3}$$

where I_0 depends on τ_f, τ_t and κ. In case of an experiment, where one wants to fit this function to real data, the limited time resolution of the detection system has to be taken into account by a convolution of $W(t)$ with the resolution function. This will be discussed in more detail during the analysis of this experiment.

For more details on the theoretical background of positron annihilation, we refer the reader to [3].

1.2 Measurement Devices

1.2.1 Full fast-slow Coincidence Circuit

The *fast-slow coincidence circuit* is the setup used to measure the lifetime of positrons in this experiment, it is shown in figure 2.7. The fast circle measures the time and is controlled by the slow circle, identifying the events.

Two LYSO scintillators connected to photomultipliers are used to detect the photons from the sample. In the slow circle, the pulses from the dynodes of the photomultipliers are amplified and analysed by SCA's identifying the 1275 keV and 511 keV signals. A coincidence unit determines whether the outputs of the SCA's

are coincident in time, which means overlapping in a certain time scale.

The fast circle takes the signal of the anode of the photomultiplier to CFD's, which then trigger the TAC's start and stop respectively. The downstream MCA creates a histogram of the such measured lifetime. With the coincidence unit, it is possible to sort out coincident events by enabling the MCA.

Additional theory on the measurement devices can be found in the appendix A.

2 Experimental Analysis

2.1 Experimental Setup

In order to be able to measure the lifetime of the positron, we have to adjust the experimental set up such that we can measure the 1275 keV start signal with one and the 511 keV stop signal with the other detector. This includes setting up the slow circuit, adjusting the fast circuit and doing a time calibration measurement.

2.1.1 Setting up the slow circuit

In the first part of the experiment, we have to set up the slow circuit for both of the detectors in order to identify the energy peaks in the spectrum and adjust the windows of the SCA's. The detectors are each set up as shown in figure 2.1.

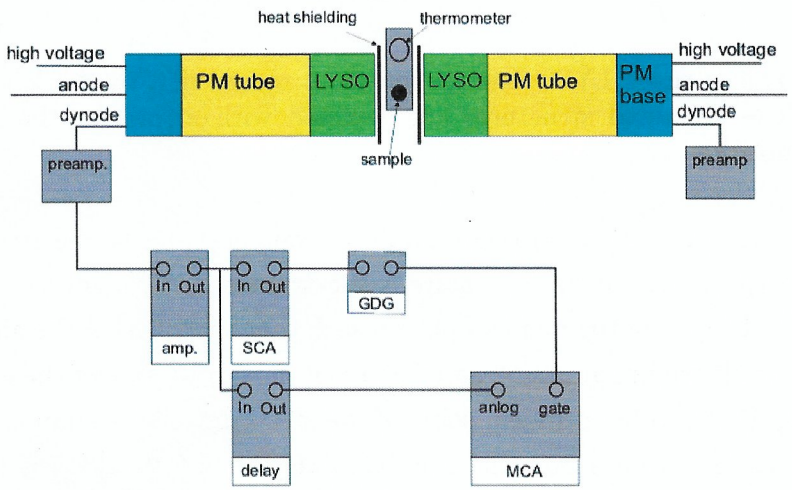

Figure 2.1.: Scheme of the detector setup for the slow circuit of one detector, taken from [4].

We use the output of the SCA as a gate for the MCA and check its signal for simultaneousness with the analogue signal peak (delay...). Once set up properly, we record an intrinsic LYSO energy spectrum for both detectors. What we find for the left detector is depicted in figure 2.2, the right detector yields the same spectrum.

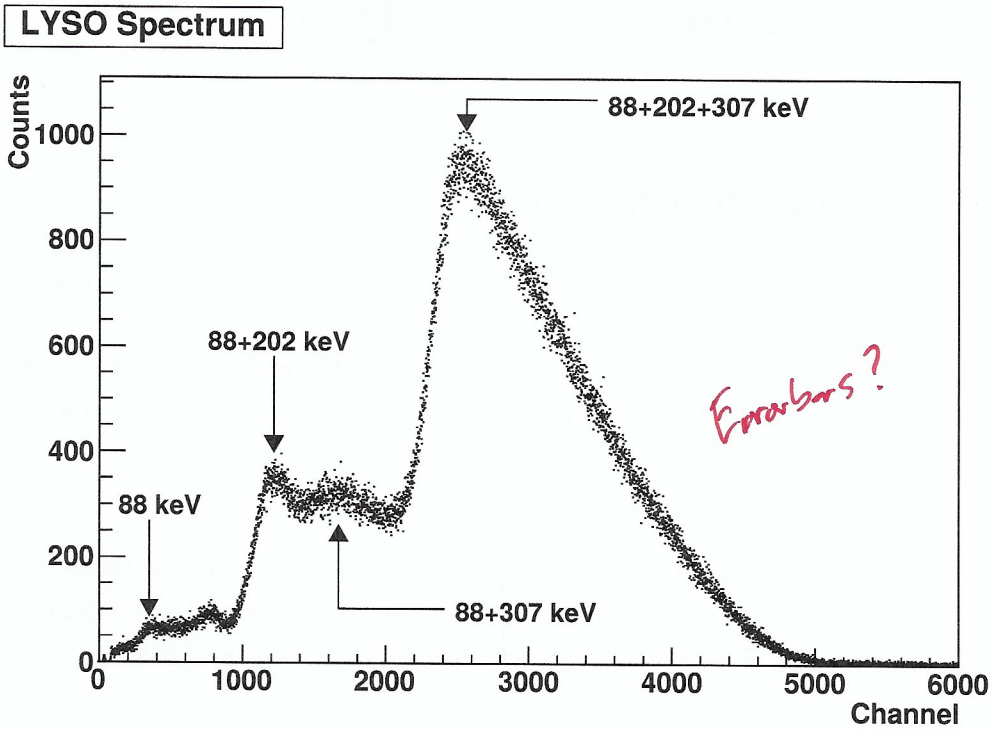

Figure 2.2.: The intrinsic LYSO energy spectrum recorded with the left detector. The identified structures are depicted with arrows at the respective position.

Using figure A.1 and the fourth reference in [1], we can identify the structures as shown in the spectrum. We also acquire a spectrum of a ^{22}Na source, where we have to adjust the gain of the main amplifiers such that the 1275 keV line is covered. What we find is shown in figures 2.3 and 2.4. Even though we expect the same spectrum as in figure 2.2 to be included, some of the structures are overlapped and not visible. The additional lines from the e^-e^+-annihilation in ^{115}In and the relaxation of ^{22}Ne are depicted in figures 2.3 and 2.4.

Before setting up the fast circuit, we prepare the setup for the time calibration measurement. This means setting cuts on the channels of the left and right detector (i.e. adjust the SCA windows) such that the 511 keV γ-rays simultaneously emitted from the e^-e^+-annihilation are detected. The applied cuts are also depicted in

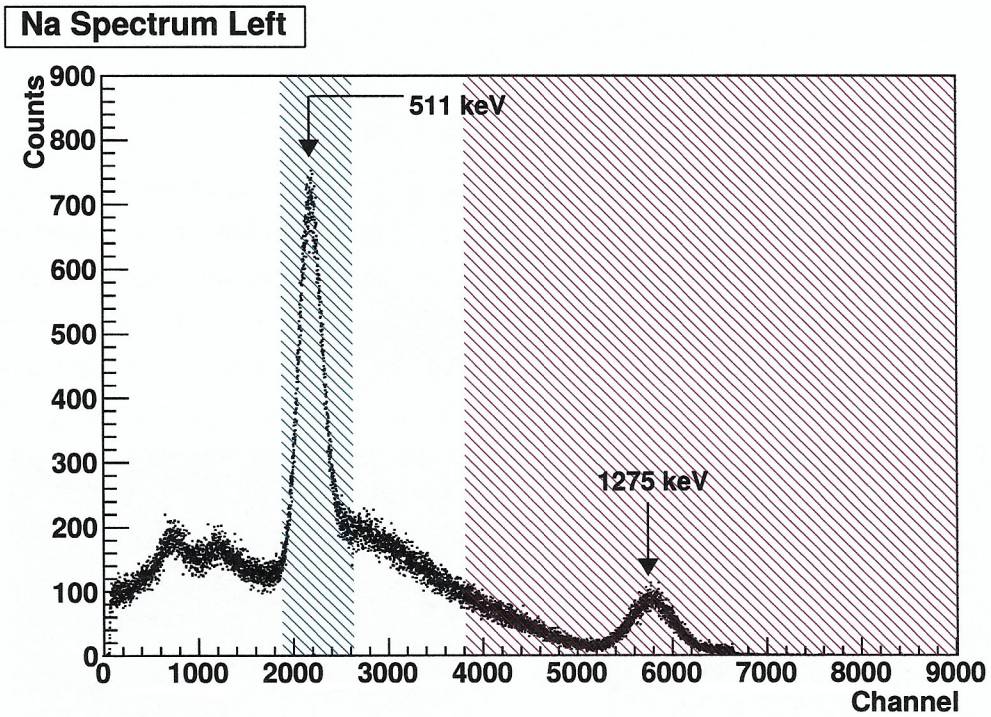

Figure 2.3.: The energy spectrum of the Na-Source recorded with the left detector.

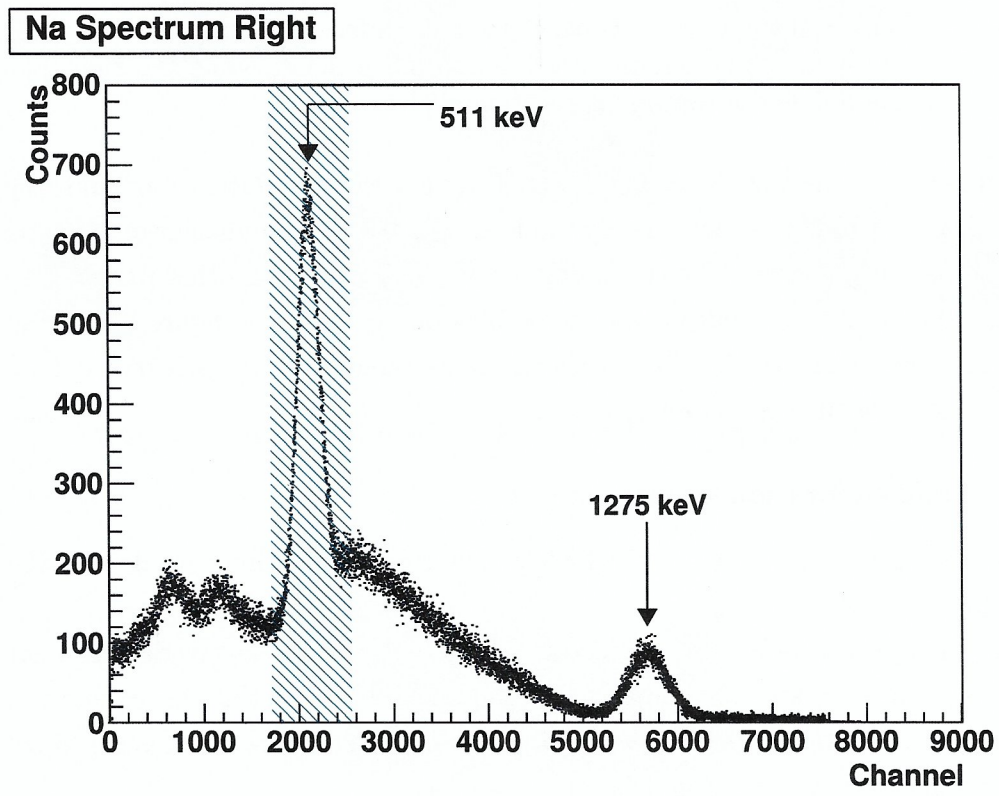

Figure 2.4.: The energy spectrum of the Na-Source recorded with the right detector.

figures 2.3 and 2.4 as the blue shaded area.

2.1.2 Adjustment of the fast circuit

For the time calibration measurement, we furthermore have to adjust the thresholds of the CFD's in the fast circuit of both detectors. The thresholds are supposed to be as low as possible with a good acceptance, yet cut away noise appropriately. The result displayed on the oscilloscope is shown in figure 2.5, where the left picture has too much noise and the right picture has just the right settings to fulfill these conditions.

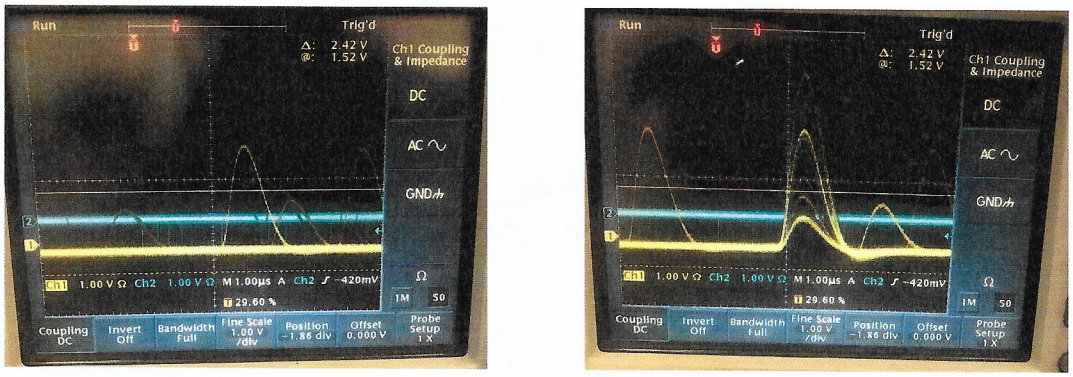

Figure 2.5.: The display of the oscillator for two different settings of the CFD thresholds. The left picture has too much noise, while the right picture fulfills the conditions mentioned above.

What is to be done now, is setting a time delay between the (later) start and stop signal of ca. 20 ns. Here, we already made use of the delay unit shown in figure 2.8 with a setting of 8 ns. The remaining delay is adjusted with other parts of the experimental setup. The output on the oscilloscope is shown in figure 2.6. After connecting the signals to the TAC (with the same cables, due to their own delay), the time range of the TAC is set to 50 ns.

2.1.3 Time calibration measurement

We now set up the experiment with the fast-slow-coincidence circuit as depicted in figure 2.7.
After checking the SCA's, TAC's and coincidence outputs of the two detectors for simultaneousness, we are able to measure prompt curves and do the time calibration measurement. We therefore start with the delay unit (see figure 2.8) having '8 ns' turned on and increase the stop delay in steps of 4 ns.
To ensure a statistical uncertainty of less than 1 %, we then measure the count rate for time intervals of 30 seconds, plot these values in a graph and fit gauss curves

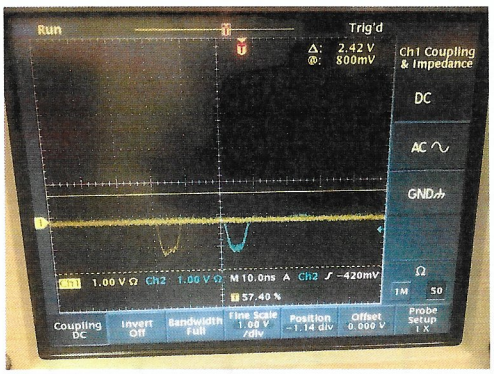

Figure 2.6.: The display of the oscillator after adjusting the delay between start and stop signal to 20 ns.

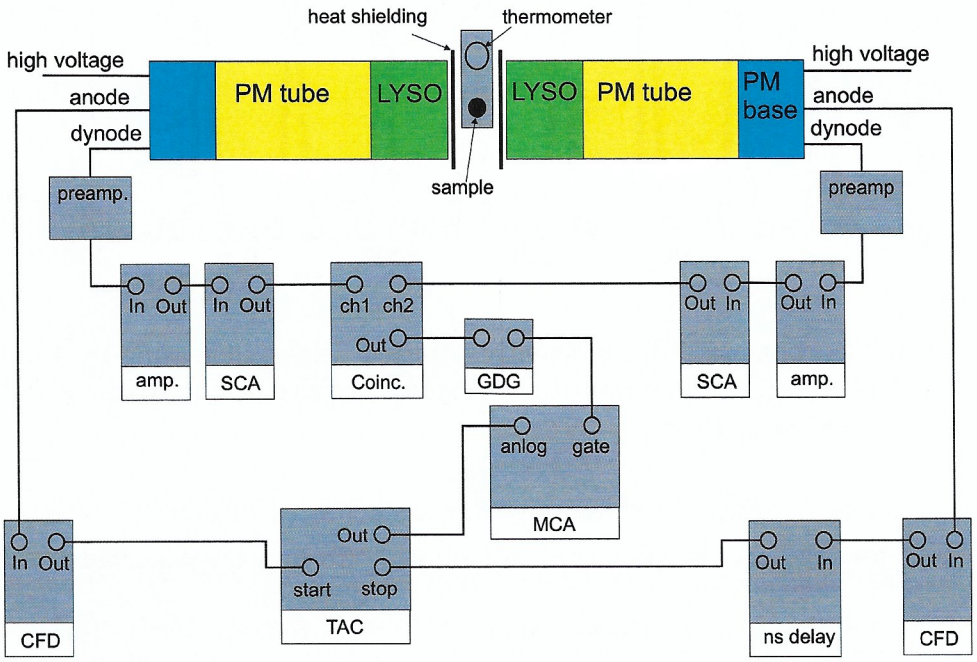

Figure 2.7.: Scheme of the fast-slow-coincidence circuit, taken from [4].

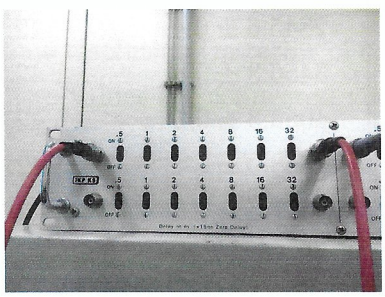

Figure 2.8.: The delay unit, having only 8 ns turned on as in the beginning of the time calibration measurement.

onto each of the resulting peaks. What we arrive at is depicted in figure 2.9, where the delay is increased from the left to the right peaks.

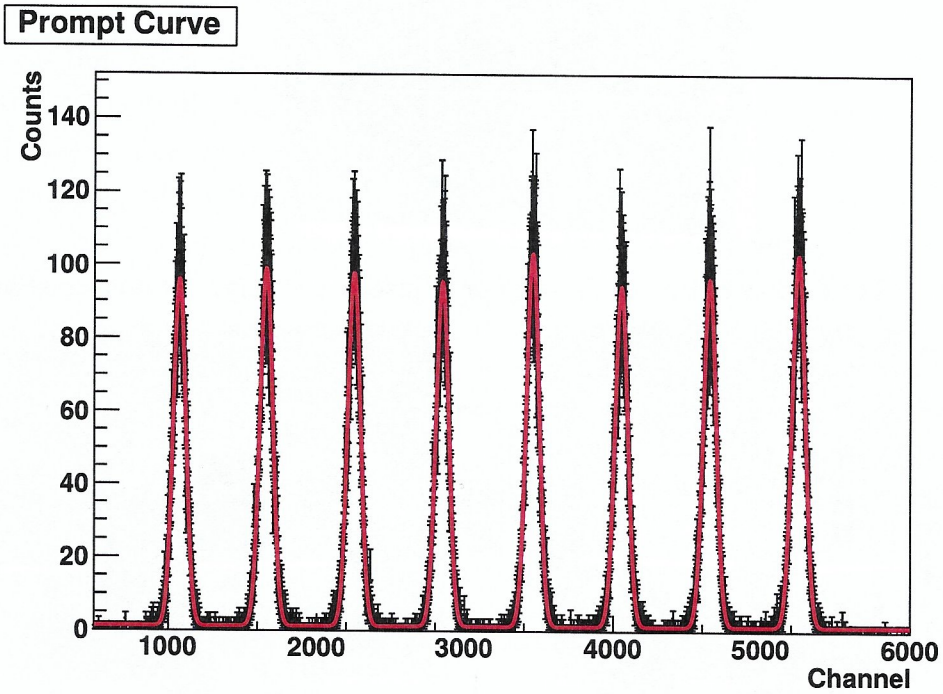

Figure 2.9.: The count rates for differently adjusted delays, increasing by 4 ns per peak from left to right with fitted gauss curves onto the peaks. $\chi^2/\text{ndf} = 2602/3511$. Prob $= 1$.

The parameters from the fitted gauss curves are collected in table 2.1 where the start value for the delay is considered to be 0 ns. To find the expected linearity

Delay in ns	Mean value μ	Stand. deviation σ
0	1072.2 ± 0.4	42.0 ± 0.3
4	1658.0 ± 0.4	42.5 ± 0.3
8	2250.4 ± 0.4	42.3 ± 0.3
12	2845.6 ± 0.4	42.2 ± 0.3
16	3456.3 ± 0.4	42.2 ± 0.3
20	4053.3 ± 0.5	42.8 ± 0.4
24	4648.0 ± 0.4	42.3 ± 0.3
28	5247.3 ± 0.4	42.9 ± 0.3

Table 2.1.: Parameters obtained for the fitted gauss curves. We put an offset on the delay, such that the first value considered equals a delay of 0 ns.

between the channels and the time, we now plot the channels in terms of the mean

values from table 2.1 against the delay time in ns and fit a linear equation onto the values. The errors on the channels (x-axis) are assumed to be given by the standard deviations from table 2.1. We find figure 2.10 for the plot and for the linear equation

$$t(C) = (0.00669 \pm 0.00007)\,\text{ns} \cdot C - (7.11 \pm 0.25)\,\text{ns}. \tag{2.1}$$

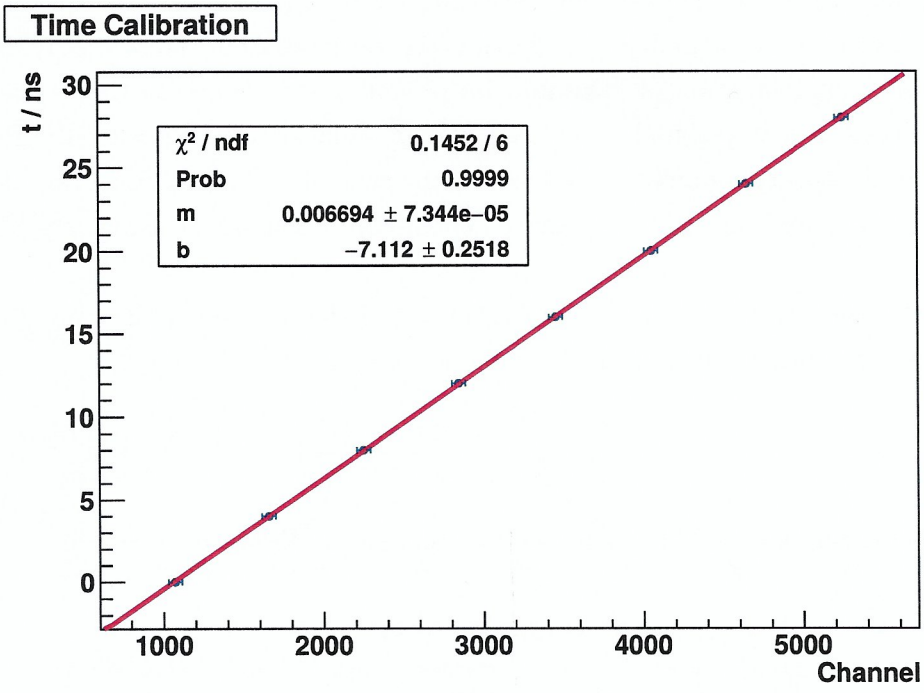

Figure 2.10.: The channels from table 2.1 plotted against the delay in ns.

To obtain the resolution of the time measurement, we calculate the weighted mean of the standard deviations from table 2.1 using eq. (B.1) and eq. (B.2) from appendix B. For this value, we find

$$\sigma_{\text{wm}} = (42.41 \pm 0.12)$$

in terms of channels. The time resolution (in terms of channels) is now given as the FWHM value, where these two values are connected via

$$\text{FWHM}_{\text{wm}} = 2\sqrt{2\ln 2}\sigma_{\text{wm}} = 99.87 \pm 0.28.$$

As we only consider differences in time, it is sufficient to use the slope of eq. (2.1) in order to find the time resolution, given by

$$\Delta t_{\text{res}} = (668.1 \pm 7.2)\,\text{ps}.$$

2.2 Lifetime Measurements

In order to measure the lifetime spectra of the positron, we set the left SCA's window to the 1275 keV line. This can be seen in figure 2.3 as the red shaded area, where we also included part of the compton background. The right SCA's window is left untouched, cutting for the 511 keV line in the spectrum. The 1275 keV line can then be used as a start pulse, signalizing the birth of the positron from the β^+-decay due to the subsequent relaxation of ^{22}Ne into its ground state. Whereas the 511 keV line can be used as a stop signal, signalizing the annihilation of the positron. After checking the SCA outputs and the fast-slow coincidence for simultaneousness once more, we are prepared for the temperature dependent measurement using the ^{115}In sample.

During the analysis of this part, we fit functions of the form eq. (1.3) convolved with the time resolution function of the detection system

$$P(t) = \frac{1}{\sqrt{2\pi}\sigma} \exp\left(-\frac{1}{2}\frac{(t-t_0)^2}{\sigma^2}\right)$$

onto the measured values. This results in a fit function of the form

$$\begin{aligned} M(t) = (W * P)(t) &= \int_0^t W(p)P(p-t)\,\mathrm{d}p \\ &= \frac{A_0}{2\tau_0} \exp\left(\frac{\sigma^2 - 2\tau_0(t-t_0)}{2\tau_0^2}\right)\{erf(a_0) + erf(b_0)\} \\ &+ \frac{A_t}{2\tau_t} \exp\left(\frac{\sigma^2 - 2\tau_t(t-t_0)}{2\tau_t^2}\right)\{erf(a_t) + erf(b_t)\} + \text{'BG'} \end{aligned} \tag{2.2}$$

for the measured lifetime spectrum. Here,

$$\begin{aligned} a_0 &= \frac{\sigma^2 + \tau_0 t_0}{\sqrt{2}\sigma\tau_0}, & b_0 &= \frac{\tau_0(t-t_0) - \sigma^2}{\sqrt{2}\sigma\tau_0}, \\ a_\mathrm{t} &= \frac{\sigma^2 + \tau_\mathrm{t} t_0}{\sqrt{2}\sigma\tau_\mathrm{t}}, & b_\mathrm{t} &= \frac{\tau_\mathrm{t}(t-t_0) - \sigma^2}{\sqrt{2}\sigma\tau_\mathrm{t}} \end{aligned} \tag{2.3}$$

contain the fit parameters σ, t_0, τ_0 and τ_t. Furthermore,

$$I_0 = \frac{A_0}{A_0 + A_\mathrm{t}}, \qquad I_\mathrm{t} = \frac{A_\mathrm{t}}{A_0 + A_\mathrm{t}} \tag{2.4}$$

contain the fit parameters A_0 and A_t,

$$erf(x) = \int_0^x e^{-y^2}\,\mathrm{d}y$$

is the error function and 'BG' the background.

The first lifetime spectrum we record is at room temperature (= 299.0 K) for 20 minutes. The resulting plot with its fitted parameters is shown in figure 2.11.

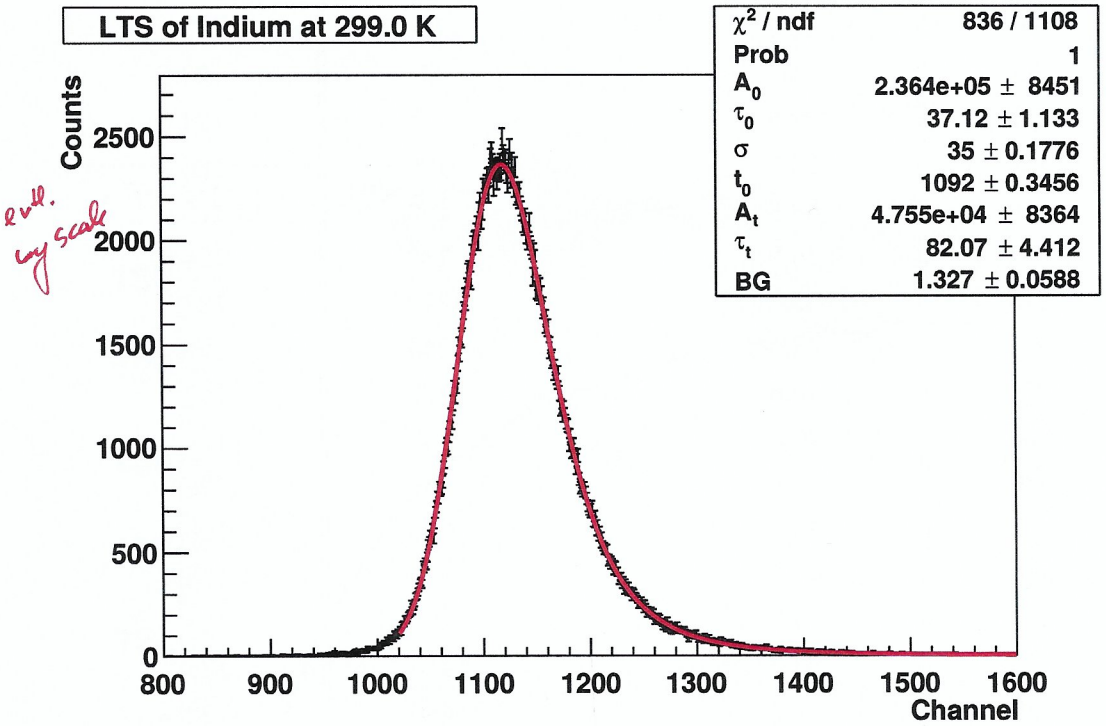

Figure 2.11.: The lifetime spectrum for the ^{155}In sample at $T = 299.0\,\mathrm{K}$.

Heating the sample up from 299.0 K to 326.4 K, we also measure its temperature every 30 seconds in order to find the time constant of the heating system. By doing this, we will be able to set reasonable heating powers on the potentiometer and estimate the time needed for the system to stabilize in between 1 K. What we find is depicted in the left table of 2.2 and the corresponding plot is given as the red curve in figure 2.12. A second measurement of the same kind is done for the heating from 395.3 K to 402.7 K. The resulting values can be found in the right table of 2.2 and the corresponding plot is given as the blue curve in figure 2.12. Noticeable is here, that the two curves have the same behavior, independent of the temperature region and difference. Yet, the blue curve stabilizes more quickly in between 1 K. We thus draw the connection, that this coincides with the smaller temperature difference upon heating for the the measurement of the blue curve. As we will never increase the potentiometer by more than 150 °C, we can be positive that the system stabilizes at the latest after 12 minutes.

Before continuing the measurement, we try to optimize the count rate of the detectors by adjusting the position of the sample in the sample holder. The activity

Time t in s	Temp. T in °C
0	26.0
30	27.7
60	31
90	33.9
120	36.5
150	38.9
180	40.9
210	42.7
240	44.3
270	45.6
300	46.8
330	47.8
360	48.7
390	49.5
420	50.1
450	50.6
480	51.2
510	51.6
540	52.0
570	52.3
600	52.6
630	52.9
660	53.1
690	53.3
720	53.4
750	53.6
780	53.7
810	53.8
840	53.9
870	54.0
900	54.1

Time t in s	Temp. T in °C
0	122.2
30	122.8
60	123.7
90	124.6
120	125.3
150	126.0
180	126.5
210	127.0
240	127.4
270	127.7
300	128.0
330	128.2
360	128.4
390	128.6
420	128.7
450	128.8
480	128.9
510	129.0
540	129.1
570	129.2
600	129.2
630	129.3
660	129.3
690	129.4
720	129.4
750	129.4
780	129.5
810	129.5
840	129.5
870	129.5
900	129.5

Table 2.2.: The time and temperature values for the determination of the heating system's time constant. We set the potentiometer from 0 to 150 °C for the left table and from 400 to 450 °C for the right table.

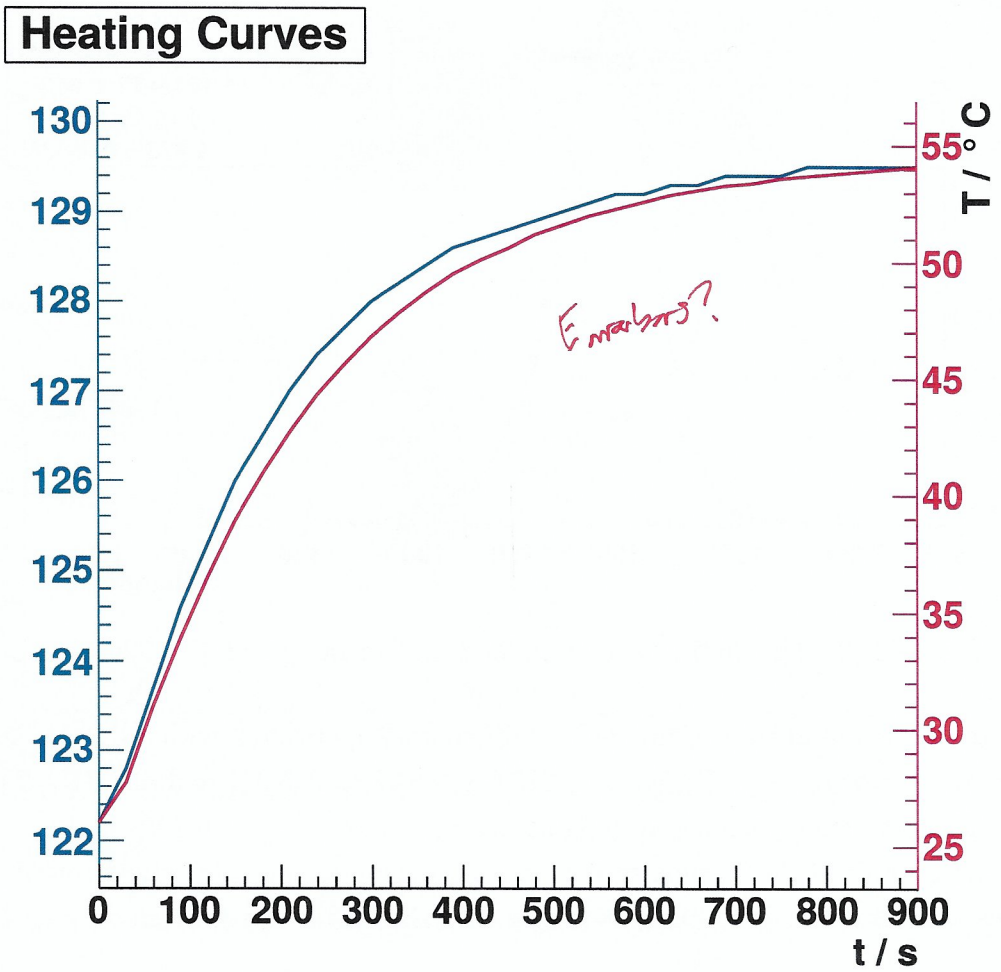

Figure 2.12.: The time plotted against the temperature for the values in table 2.2 and the resulting heating curves.

increased from $200\,s^{-1}$ to $600\,s^{-1}$ such that the tutor authorized us to decrease the time measurement from 20 minutes to 15 minutes. The next lifetime spectrum was recorded for a temperature of 326.4 K and can be found in figure 2.13.

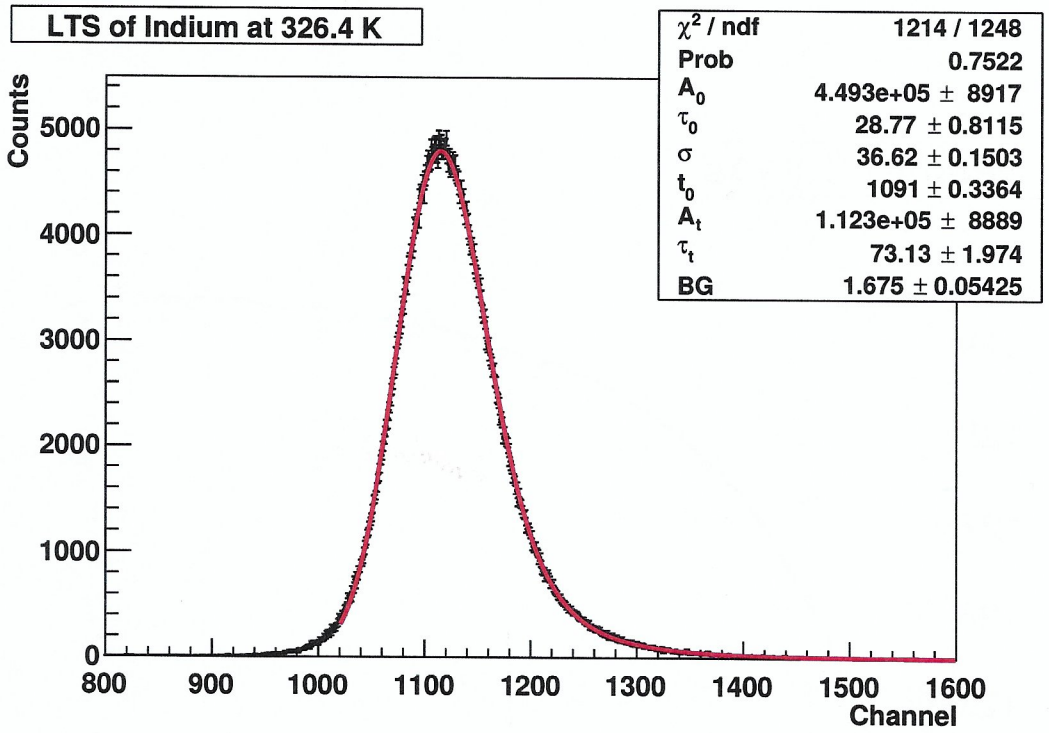

Figure 2.13.: The lifetime spectrum for the ^{155}In sample at $T = 326.4\,\mathrm{K}$.

In total, we took eight measurements at different temperatures, with the remaining temperatures being 346.4 K, 361.5 K, 370.6 K, 382.8 K, 395.3 K and 402.7 K. The lifetime spectrums can be found in figure 2.14.

Having obtained the lifetime spectra, we need some further theoretical considerations and formulas to continue with the analysis. We define a mean lifetime by

$$\bar{\tau} = I_0\tau_0 + I_t\tau_t = \tau_f\frac{1+\sigma c_t\tau_t}{1+\sigma c_t\tau_f} \tag{2.5}$$

and use the temperature dependent concentration of vacancies

$$c_t = \exp\left(\frac{S_t}{k_B}\right)\exp\left(\frac{-H_t}{k_B T}\right) \tag{2.6}$$

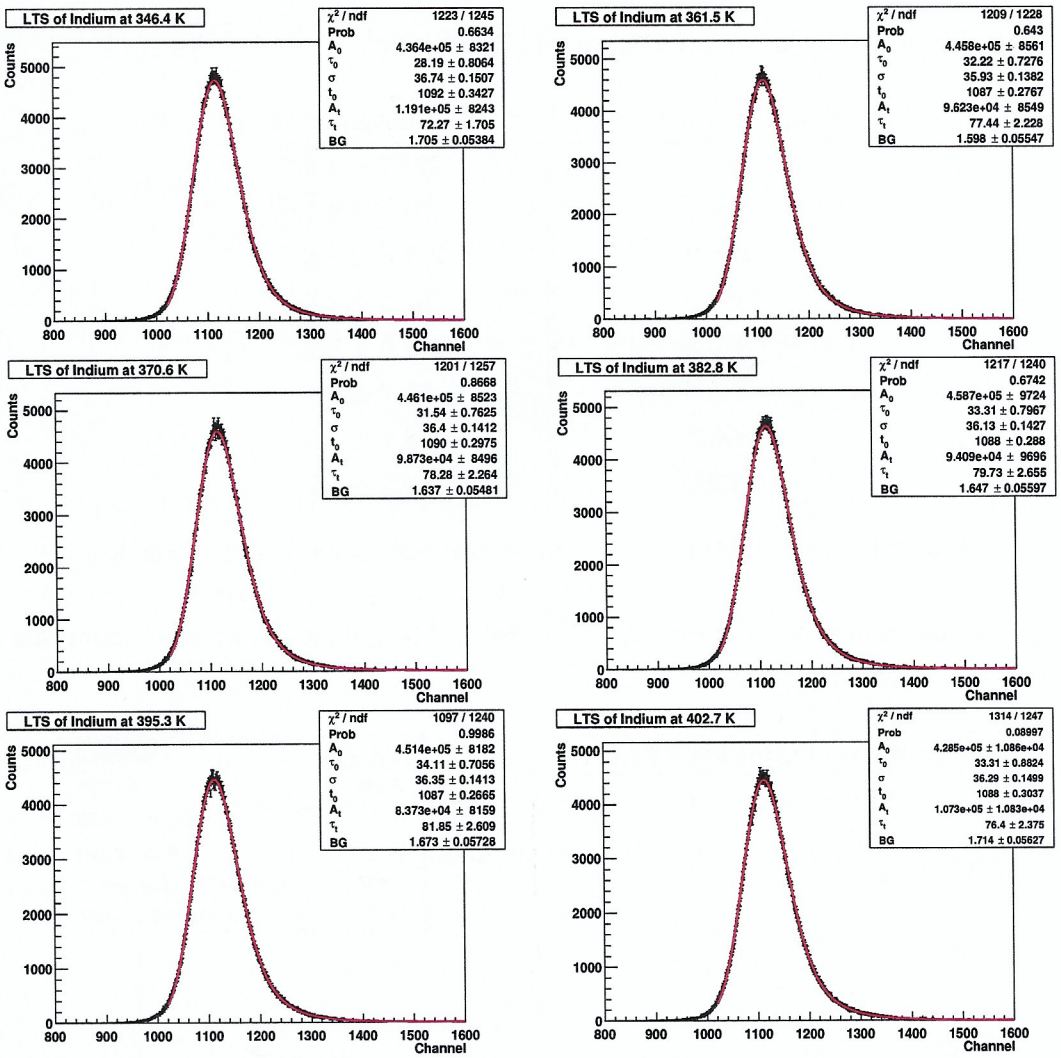

Figure 2.14.: The lifetime spectrum for the ^{155}In sample at $T = 346.4\,\mathrm{K}$, $T = 361.5\,\mathrm{K}$, $T = 370.6\,\mathrm{K}$, $T = 382.8\,\mathrm{K}$, $T = 395.3\,\mathrm{K}$ and $T = 402.7\,\mathrm{K}$.

to find an s-curve temperature dependence of the form

$$\bar{\tau} = \tau_\mathrm{f} \frac{1 + \sigma \exp\left(\frac{S_\mathrm{t}}{k_\mathrm{B}}\right) \exp\left(\frac{-H_\mathrm{t}}{k_\mathrm{B} T}\right) \tau_\mathrm{t}}{1 + \sigma \exp\left(\frac{S_\mathrm{t}}{k_\mathrm{B}}\right) \exp\left(\frac{-H_\mathrm{t}}{k_\mathrm{B} T}\right) \tau_\mathrm{f}}. \tag{2.7}$$

Here, k_B is the Boltzmann constant, S_t the vacancy formation entropy and H_t the vacancy formation enthalpy.

Using eqs. (2.4), the fitted parameters for the lifetime spectra in figures 2.11-2.14 and eq. (2.5), we can determine I_0, I_t and the mean lifetime $\bar{\tau}$ for the different temperatures. What we find is given in table 2.3, where we already used the linear

eq. (2.1) in order to convert the channels into a time.

Temperature T in K	Mean Lifetime $\bar{\tau}$ in ps
299.0	298.7 ± 2.6
326.4	251.8 ± 4.1
346.4	251.8 ± 3.6
361.5	269.3 ± 3.6
370.6	267.6 ± 3.5
382.8	275.7 ± 3.6
395.3	278.1 ± 3.6
402.7	280.5 ± 3.7

Table 2.3.: The mean lifetimes $\bar{\tau}$ for the measured temperatures of the sample.

Plotting the values for the temperature in table 2.3 against the corresponding lifetimes $\bar{\tau}$, we find figure 2.15.

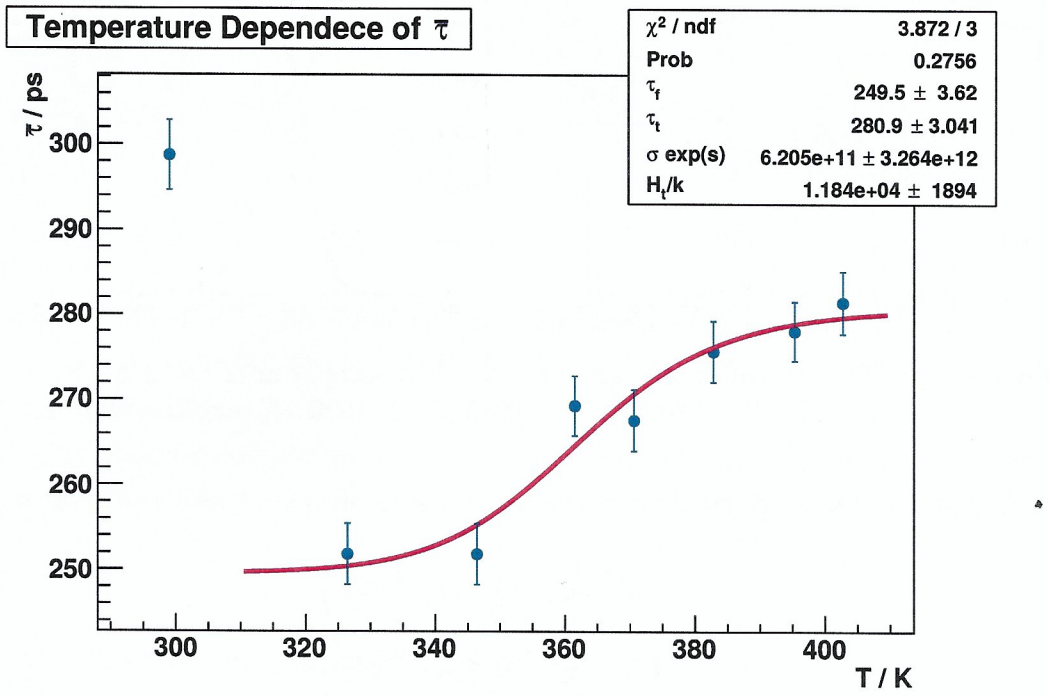

Figure 2.15.: The temperature values in table 2.3 plotted against the corresponding lifetimes $\bar{\tau}$ with the fitted s-curve of the form eq. (2.7).

Here, we also fitted an s-curve of the form eq. (2.7) to the values in order to determine

$$\tau_f = (249.50 \pm 3.62)\,\text{ps}.$$

Compared to the literature value (see [1, p.60 et seqq.])

$$\tau_{\mathrm{f}}^{\mathrm{lit}} = 193\,\mathrm{ps},$$

our value is clearly larger without us having an explanation for this. This also matches the shift of $\bar{\tau}$ of $\sim 50\,\mathrm{ps}$ compared to the literature (see [1, p.60]). Furthermore, the fitted parameter for τ_{t} is clearly smaller than the values for τ_{t} determined from the lifetime spectra but fits better to the literature value (see [1, p.62])

$$\tau_{\mathrm{t}}^{\mathrm{lit}} = 264\,\mathrm{ps}.$$

The fit parameter $\sigma \exp(s)$ contains the defined variable $s \equiv \frac{S_{\mathrm{t}}}{k_{\mathrm{B}}}$. Note also, that we excluded the first datapoint (room temperature $T = 299.0\,\mathrm{K}$) from the fit due to its strong deviation from the expected s-curve behavior.

Rewriting eq. (2.5) to

$$\sigma c_{\mathrm{t}} = \frac{\bar{\tau} - \tau_{\mathrm{f}}}{\tau_{\mathrm{f}}(\tau_{\mathrm{t}} - \bar{\tau})}, \tag{2.8}$$

we calculate $\ln(\sigma c_{\mathrm{t}})$ for the measured temperatures, where we used the values for τ_{f} and τ_{t} from the fitted s-curve in figure 2.15. The said values can be found in table 2.4, where we excluded the first datapoint $T = 299.0\,\mathrm{K}$ (room temperature).

$1/T$ in $1/K$	$\ln(\sigma c_{\mathrm{t}})$ in $\ln(1/ps)$
0.003063 ± 0.000005	-8.05 ± 2.43
0.002887 ± 0.000004	-8.06 ± 2.29
0.002767 ± 0.000004	-4.99 ± 0.59
0.002698 ± 0.000004	-5.21 ± 0.55
0.002613 ± 0.000003	-3.90 ± 1.02
0.002530 ± 0.000003	-3.18 ± 1.81
0.002483 ± 0.000003	-1.08 ± 13.14

Table 2.4.: The inverse temperatures $1/T$ with the corresponding value for $\ln(\sigma c_{\mathrm{t}})$ obtained from eq. (2.8).

Using table 2.4, we now plot $\ln(\sigma c_{\mathrm{t}})$ against $1/T$ – a so-called Arrhenius Diagram – in order to determine the vacancy formation enthalpy H_{t}. The connection between these values is given by eq. (2.6), which can be rewritten as

$$\ln(\sigma c_{\mathrm{t}}) = -\frac{H_{\mathrm{t}}}{k_{\mathrm{B}}}\frac{1}{T} + \frac{S_{\mathrm{t}}}{k_{\mathrm{B}}} + \ln\sigma. \tag{2.9}$$

The plot with the fitted function and the parameters of the fit can be found in figure

2.16.

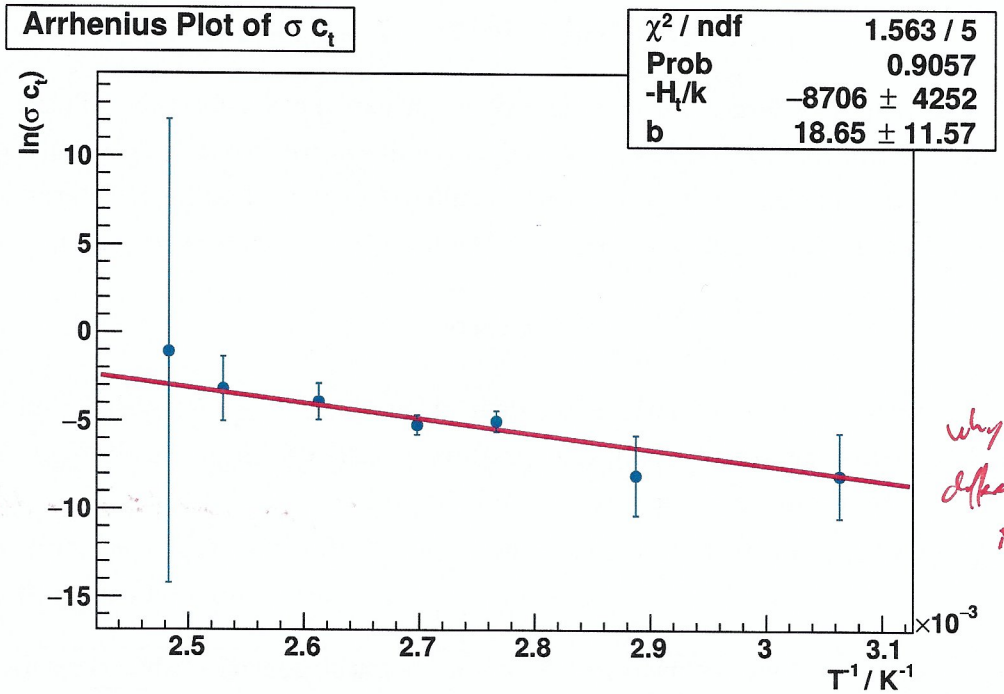

Figure 2.16.: The inverse temperature values in table 2.4 plotted against the corresponding values $\ln(\sigma c_t)$ with the fitted function of the form eq. (2.9).

Inserting the Boltzmann constant and converting to eV, we find the vacancy formation enthalpy

$$H_t = (0.75 \pm 0.37)\,\text{eV}. \tag{2.10}$$

Even though this value is in the 1σ confidence level of the literature value (see [1, 56])

$$H_t^{\text{lit}} = (0.54 \pm 0.003)\,\text{eV}, \tag{2.11}$$

it seems a little bit off and has a large error. This could be optimized by measuring more lifetime spectra at different temperatures for a longer period of time. We try to exclude some of the datapoints for the fit and find figure 2.17.

The value for the vacancy formation enthalpy now reads

$$H_t = (0.57 \pm 0.51)\,\text{eV}.$$

The value is closer to the literature value eq. (2.11) but has a larger error than eq. (2.10).

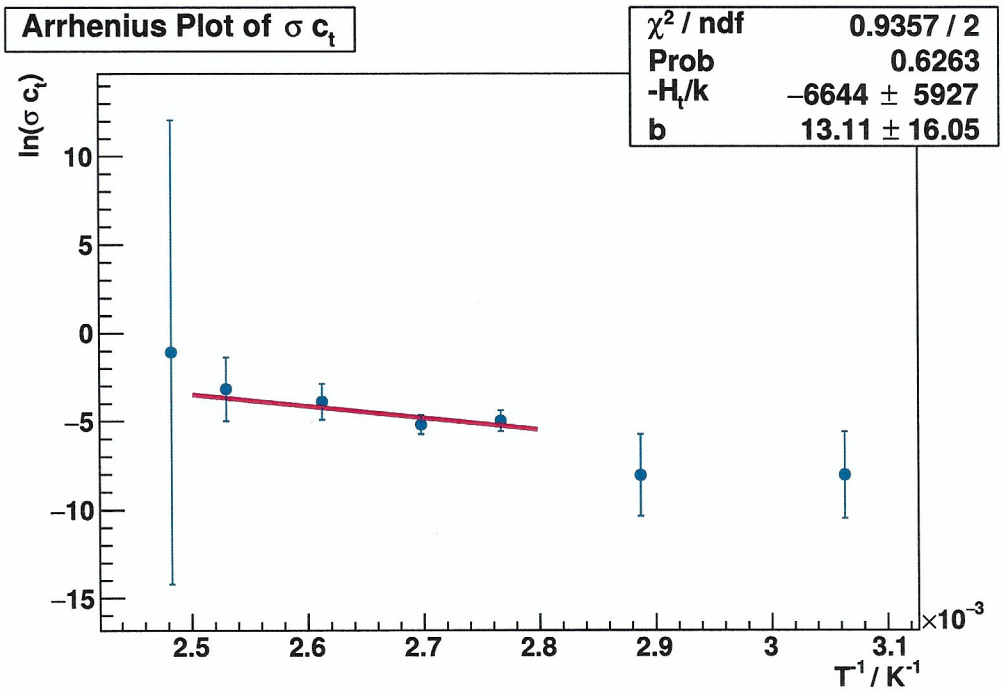

Figure 2.17.: The inverse temperature values in table 2.4 plotted against the corresponding values $\ln(\sigma c_t)$ with the fitted function of the form eq. (2.9). Here, some datapoints are left out in the fit.

2.2.1 Positronium in Acrylic glass

Due to new regulations at the University of Bonn, students are not allowed to do measurements overnight anymore. The radioactive probes can not stay in the room without either the tutor or the students performing the experiment present. For this reason, we were not able to perform the measurement with the acrylic glass sample instead of the ^{155}In sample. As the acrylic glass is not a metal, one would expect the formation of positronium in it and thus different results for the lifetime measurements as before. As a substitution for this part, our tutor suggested to do the measurement of the heatings system's time constant for two different temperature ranges. This is what can be found in the previous part of this report.

3 Conclusion

In this experiment, we measured the lifetime of positrons and the vacancy formation enthalpy in ^{155}In. After having set up the fast-slow-coincidence circuit in the first part of the experiment, we were able to confirm the linearity of the MCA's and determine the detectors time resolution to $\Delta t_{\text{res}} = (668.1 \pm 7.2)\,\text{ps}$.

In the second part of the experiment, we recorded lifetime spectra at different temperatures and additionally determined the heating system's time constant. Here, we found out that the heating behavior is independent of the temperature region. For the mean lifetime, we were able to confirm the expected s-curve temperature behavior. The determined values for $\bar{\tau}$ and $\tau_{\text{f}} = (249.50 \pm 3.62)\,\text{ps}$ are $\sim 50\,\text{ps}$ off the literature values from [1, p.60 et seq.], while the value for $\tau_{\text{t}} = (280.90 \pm 3.04)\,\text{ps}$ is closer to the literature value. The resulting value for the vacancy formation enthalpy $H_{\text{t}} = (0.75 \pm 0.37)\,\text{eV}$ could be improved to $H_{\text{t}} = (0.57 \pm 0.51)\,\text{eV}$ by leaving out some data points. Both values have large errors and are thus in the 1σ confidence level of the literature value $H_{\text{t}}^{\text{lit}} = (0.54 \pm 0.003)\,\text{eV}$. The values and corresponding errors could be improved by measuring the lifetime spectra at more temperatures and for longer periods of time. This could also improve the fit results to the lifetime spectra for τ_{f} and τ_{t}.

A Measurement Devices

A.1 LYSO scintillator

To detect the photons created by e^-e^+-annihilation in the analysed material, a *LYSO scintillator* (Lutetium-Yttrium Oxyorthosilicate) is used. A scintillator is an organic or anorganic material which emits light when ionizing radiation is passing. The photons from e^-e^+-annihilation and the 1275 keV line of the ^{22}Na-decay interact with the scintillation material via the photoelectric effect, compton scattering and pair production[1] [2].

Since the photoelectric effect is the preferred type of interaction (because all energy is deposited into the scintillator here) materials with a high atomic number Z – like Lutetium – are of advantage. The LYSO scintillator also has the advantages of a low attenuation length for 511 keV and a short decay time [1] such that it is perfectly suited for positron annihilation spectroscopy. The LYSO scintillator contains the radioactive nuclide ^{176}Lu which leads to self absorption lines in the spectra, a decay scheme is shown in figure A.1.

A.2 Photomultiplier

The light signals of the scintillator are collected by a photomultiplier. The photons hit the cathode and the cathode emits electrons which get accelerated in an electric field to the dynode. Here the electrons have enough energy to release an avalanche of secondary electrons. This process is repeated until a measurable output is created at the anode [2]. The signal at the anode might have lost its proportionality to the incoming energy. Thus it is also possible to use another dynode as the output, giving a slow rising signal (*slow-circle*) in contrast to the signal at the anode with a fast rising time (*fast-circle*).

[1] Pair production can be neglected for the photons produced by e^-e^+-annihilation.

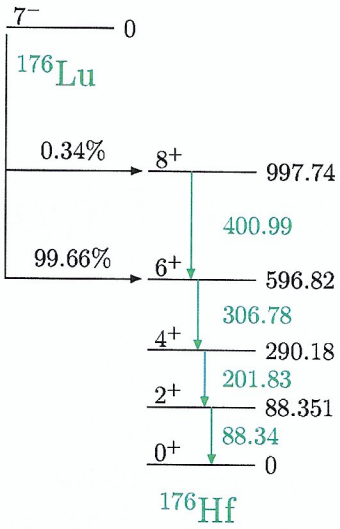

Figure A.1.: Decay scheme of ^{176}Lu, following [4].

A.3 Single Channel Analyzer (SCA) and Constant Fraction Discriminator (CDF)

A *single channel analyszer (SCA)* sorts incoming analogue signals according to their amplitude and gives a digital output. It contains a lower and upper level threshold so that only signals within this interval give a response [2].

A *constant fraction discriminator (CFD)* triggers on a fraction of the peak maximum. This yields to an independent trigger time when analyzing signals of same shape but different pulse heights, see figure A.2. CFDs are used here in the *fast circut*. In the experiment SCAs and CFDs are used to filter the 1275 keV start and the 511 keV stop signal.

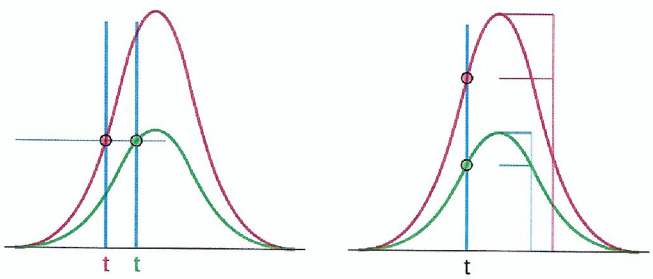

Figure A.2.: Threshold triggering (left) vs. CFD triggering (right). Taken from `https://de.wikipedia.org/wiki/Constant_Fraction_Discriminator`.

A.4 Time to Amplitude Converter (TAC) and Multi Channel Analyzer (MCA)

To measure the lifetime of the positron inside the tested material a *time to amplitude converter (TAC)* is used. It is triggered by a start pulse (1275 keV signal) and halted by a stop signal (511 keV) giving an output proportional to the passed time, e.g. by decharging a capacitor [2].

The output of the TAC is used as input for a *multi channel analyzer (MCA)*. This sorts out the incoming pulses according to their heights and increments a memory channel proportional to that value [2]. The MCA can thus create a lifetime histogram.

B Statistical Methods

Following [8], we want to summarize how to calculate a weighted mean for physical measurements. Taking N measurements $x_1, \ldots, x_N$ with errors $\epsilon_1, \ldots, \epsilon_N$, the weighted mean is defined as

$$x_{\mathrm{m}} = \frac{\sum_{i=1}^{N} w_i x_i}{\sum_{i=1}^{N} w_i} \quad \text{where} \quad w_i = \frac{1}{\sigma_i^2}. \tag{B.1}$$

The error on this mean is given by

$$\epsilon_m = \frac{1}{\sqrt{\sum_{i=1}^{N} w_i}}. \tag{B.2}$$

Peculiarly is here, that with the weights defined like this, more precise measurements count more than less precise measurements.

Bibliography

[1] University of Bonn. *Advanced Physics Laboratory Course, K225 – Additional Information handed out.* Consists of:
1. Universität Bonn, Fortgeschrittenen Praktikum, K225 – Positronenlebensdauer
2. Dissertation, Unknown Author,
https://sundoc.bibliothek.uni-halle.de/diss-online/08/08H048/t2.pdf
3. L.C. Smedskjaer and M.J. Fluss. Experimental Methods of Positron Annihilation for the Study of Defects in Metals. Materials Science and Technology Division Argonne National Laboratory Argonne, Illinois.
https://doi.org/10.1016/S0076-695X(08)60065-4.
4. Saint-Gobain Crystals. PreLude 420 Scintillation Material.

[2] W. R. Leo *Techniques for Nuclear and Particle Physics* Springer Verlag, 1987

[3] M. E. Peskin and D. V. Schroeder. *An Introduction to Quantum Field Theory.* Westview Press, 2016.

[4] University of Bonn. *Advanced Physics Laboratory Course, K225 – Further Instructions handed out.*

[5] C. Patrignani et al. (Particle Data Group), Chin. Phys. C, 40, 100001 (2016) and 2017 update.

[6] University of Bonn. *Advanced Laboratory Course (physics601), Description of Experiments: K225 Positron Lifetime in Metals and Insulators.* (Blue booklet). January 2015.

[7] RWTH Aachen, Thomas Hebbeker. Vorbereitungskurs F-Praktikum B (Physik) https://web.physik.rwth-aachen.de/~hebbeker/lectures/stat_fprakt_1.pdf.

[8] University of Colorado, Minhyea Lee. PHYS2150 Experimental Physics, Spring 2018
https://www.colorado.edu/physics/phys2150/phys2150_sp14/phys2150_lec4.pdf.